Published in final edited form as:
Biomaterials. 2010 November ; 31(33): 8596–8607. doi:10.1016/j.biomaterials.2010.07.072.

Dense type I collagen matrices that support cellular remodeling and microfabrication for studies of tumor angiogenesis and vasculogenesis in vitro

Valerie L. Cross[1], **Ying Zheng**[2], **Nak Won Choi**[2], **Scott S. Verbridge**[1], **Bryan A. Sutermaster**[2], **Lawrence J. Bonassar**[1], **Claudia Fischbach**[1], and **Abraham D. Stroock**[*,2]

[1]Department of Biomedical Engineering, Cornell University, Ithaca, NY 14853, USA

[2]School of Chemical and Biomolecular Engineering, Cornell University, Ithaca, NY 14853, USA

Abstract

Type I collagen is a favorable substrate for cell adhesion and growth and is remodelable by many tissue cells; these characteristics make it an attractive material for the study of dynamic cellular processes. Low mass fraction (1.0–3.0 mg/ml), hydrated collagen matrices used for three-dimensional cell culture permit cellular movement and remodeling, but their microstructure and mechanics fail to mimic characteristics of many extracellular matrices *in vivo* and limit the definition of fine-scale geometrical features (< 1 mm) within scaffolds. In this study, we worked with hydrated type I collagen at mass fractions between 3.0 and 20 mg/ml to define the range of densities over which the matrices support both microfabrication and cellular remodeling. We present pore and fiber dimensions based on confocal microscopy and longitudinal modulus and hydraulic permeability based on confined compression. We demonstrate faithful reproduction of simple pores of 50 μm-diameter over the entire range and formation of functional microfluidic networks for mass fractions greater than 10.0 mg/ml. We present quantitative characterization of the rate and extent of cellular remodelability using human umbilical vein endothelial cells. Finally, we present a co-culture with tumor cells and discuss the implications of integrating microfluidic control within scaffolds as a tool to study spatial and temporal signaling during tumor angiogenesis and vascularization of tissue-engineered constructs.

1 Introduction

Biologists and engineers have developed three-dimensional (3-D) scaffolds to create functional tissues for regenerative medicine [1] and study basic tissue-scale biology [2] and development [3]. The vascular cell biology community has exploited 3-D biomaterials *in vitro* in an effort to mimic the microenvironment of stromal and tumor cells *in vivo*. More specifically, 3-D scaffolds have served for the study of mechanisms of tumor metastasis[4], chemical signaling during tumor angiogenesis[5], and the vascularization of tissue engineered implants[6]. The chemistry and mechanics of extracellular matrix (ECM) significantly influence cell differentiation, proliferation, migration, shape, and biosynthetic activity [7–10]. In order to influence these responses, the biomaterial community has focused on controlling mechanical

[*]Corresponding author: Tel.:1-607-255-4276; Fax: 1-607-255-9166 ads10@cornell.edu.

[11], biological[12], and structural [13] properties of biomaterials as well as tailoring the ECM chemistry of biomaterials [14].

Recent efforts have also aimed to unite tailored biomaterial properties with microfabrication to embed micro-physiological detail with scaffolds. For example, Choi et al. fabricated microfluidic networks within mechanically robust calcium alginate hydrogels to deliver signaling factors to cells embedded within the bulk of the hydrogel [15]. These microfluidic biomaterials allow precise control over the spatial and temporal delivery of soluble factors to cells on the micrometer scale and have advanced 3-D cell culture scaffolds capabilities; however, calcium alginate is not remodelable by endothelial cells. Incorporation of chemical and physical details of the micro-scale cellular environment present *in vivo* without compromising cellular remodelability and the material's proteolytic degradation potential remains a challenge. The work described in this paper aims to overcome this limitation with the development and characterization of a dense matrix of type I collagen that both permits remodeling by endothelial cells and support perfusion through embedded microfluidic networks.

Type I collagen is abundant and has been used extensively in different forms for cell culture and tissue engineering applications [16–18]. Elsdale and Bard pioneered the use of cell-embedded native collagen gels [17]. Because collagen is 1) a natural substrate for multiple cell types, 2) remodelable by cells, and 3) easy to obtain, scientists have developed methods for using type I collagen as a tissue engineered substitute. Biologists and engineers have performed repair of nerve[19] and heart muscle [20], assays of vascular invasion and vasculogenesis [21], assays of gel contraction [22], and studies of tumor biology [23] in native type I collagen gels at low concentration (~0.3 v%). A major drawback to using conventional collagen gels for tissue engineering applications, however, is the material's weak bulk mechanical strength [24]. Contraction of the gel by constituent cells is significant[25], and its low modulus makes molding constructs into desired shapes difficult. Furthermore, in many cases, low mass fraction collagen matrices do not capture the properties of *in vivo* ECM[26].

In addition to the lithographic methods for creating the alginate microfluidic biomaterial, several research groups have developed a variety of 3-D microfabrication methods in collagen matrice [3,27,28]. Notably, Nelson et al. have developed a micromolding method by which they mold collagen solution at ≤ 3.66 mg/ml around a micropatterned PDMS stamp and construct 3-D microscale cavities embedded in collagen [3]. To create more intricate microstructure within soft materials, researchers have demonstrated that 6.5 mg/ml collagen can support 3-D microfabrication, endothelial cell attachment, and perfusion [28,29]. While these studies resulted in functional microchannels within type I collagen, the complexity and functionality of the microfabricated network with the methods used are limited because of the weak mechanical properties of the collagen.

To address the limitations mentioned above, others have used various cross-linking and denaturing processes to change the mechanical properties of collagen matrices to control the microstructure or macroscopic shape or to provide additional binding sites or signaling cues for cells. Scientists have performed both chemical and mechanical modifications of collagen by addition of glycosaminoglycans (GAGs), fibrin, and other materials [30,31]. Yannas and Burke developed and optimized crosslinked collagen-GAG membranes for skin tissue engineering [30], and, more recently, others have created these types of membranes for cell support with perfusion [32]. While these methods increase the bulk modulus or tensile strength of the collagen material, the processing also changes the chemical and molecular nature of the collagen protein. In many cases, when the triple helical structure of the collagen molecule is disrupted, the capacity for cellular degradation decreases [33]. Crosslinking methods can also be toxic to cells; and therefore, cannot be used when suspending cells in the bulk of the material.

To increase the modulus and density of collagen scaffolds without changing the native collagen molecule, Ramanujan et al. have made high concentration collagen scaffolds of 10–45 mg/ml via ultracentrifugation for studies related to diffusion and transport in tumors [26]. Also, others have created collagen scaffolds of 40 mg/ml via evaporation methods [34] for studies of fibroblast traction and migration. We build on this work on high mass fraction matrices with a systematic study of the structural and mechanical properties of dense collagen matrices and cellular interactions with them as a function of density.

Biological assays of vascular processes in 3-D do not typically employ high mass fraction native collagen matrices, and existing studies have not performed a systematic evaluation of the ability of dense collagen to promote cellular attachment, morphogenesis, and degradation or of the material's bulk mechanical characteristics. We believe dense, native collagen matrices hold promise as substrates for studies of vascular biology and as useful biomaterial for the formation of remodelable microfluidic devices. Here, we describe our methods for preparing dense collagen matrices and characterize the physical and mechanical properties of the dense type I collagen matrices (up to a collagen concentration of 20 mg/ml). We fluorescently label collagen fibers and directly compare the resolution of confocal fluorescent and confocal reflectance microscopy. Further, we report on the use of dense type I collagen as a 3-D scaffolds for the study of endothelial cell (EC) biology (EC network formation and invasion [35]), tumor angiogenesis [36], and microfabrication. We present 1) the replication of micropores in a 1.5 mg/ml (0.15%) collagen matrix, 2) methods to fabricate a functional microfluidic network within a 10 mg/ml (1%) collagen matrix, 3) evaluation of remodeling of the dense collagen by human umbilical vein endothelial cells (HUVECs), and 4) a preliminary *in vitro* model of tumor angiogenesis. Finally we discuss the implications and ongoing work of integrating microfluidic control within remodelable collagen scaffolds as a tool to study spatial and temporal signaling during tumor angiogenesis and vascularization of tissue engineered constructs.

2 Materials and Methods

2.1 Reagents

Human umbilical vein endothelial cells (HUVECs), Medium 199 (M199), fetal bovine serum (FBS), L-glutamine, penicillin/streptomycin, trypsin/EDTA, HEPES buffered saline solution (Lonza, Basel, Switzerland, formerly Cambrex). Endothelial cell growth supplement (ECGS), vascular endothelial cell growth factor (VEGF), basic fibroblast growth factor (FGF), phosphate buffered saline (PBS) (Upstate Cell Signaling Solutions, Lake Placid, NY). Rat tails (Pel-Freez Biologicals, Rogers AR). Phorbol-12-myristate-13-acetate (TPA), (Cell Signaling Technology, Danvers, MA). (poly)ethylenimine (PEI) and (tridecafluoro-1,1,2,2-tetrahydrooctyl)-1-trichlorosilane, (Sigma-Aldrich, St. Louis, Missouri). Alexa Fluor 488 phalloidin, Alexa Fluor 568 phalloidin, 4',6-diamidino-2-phenylindole (DAPI), YOYO-1 iodide, tetramethylrhodamine-5-(and-6)-isothiocyanate (TRITC) (Molecular Probes, Eugene, OR). L-ascorbic acid (Acros Organics, Atlanta, GA). Triton X-100 (MP Biomedical, Solon, OH). (poly)-dimethylsiloxane (PDMS) (Sylgard® 184, Dow Corning, Midland, Michigan). Fluoresbrite™ Carboxylate YG 1.0 micron microspheres (Polyscience, Inc., Warrington, Pennsylvania).

2.2 Collagen Gels

2.2.1 Preparation of high weight percent acidic collagen solution—Two stocks of collagen were prepared and used for all experiments described here. As described previously [37], tendons were excised from rat tails, suspended with 100 ml of 0.1% acetic acid/gram of tendon. After 48 hours at 4°C, the collagen solution (still containing bits of fat and facia) was centrifuged for 90 minutes at 8800 ×g at 4 °C in a Hettich Universal 320R bench top centrifuge (Hettich, Beverly, MA). The top, clear collagen solution was collected and the pellet was

discarded. The collagen solution was then lyophilized, and the dry mass was determined. For each stock prepared, we processed 25 tails. After the lyophilization step, we generally had high yields (~ 0.15 grams purified collagen/tail) of dry collagen.

The dried collagen was resuspended in 0.1% acetic acid at four different stock solution concentrations: 8mg/ml, 15 mg/ml, 20 mg/ml, and 30 mg/ml. To re-dissolve the lyophilized material, the suspensions were agitated approximately 3 times a day by manually inverting the tubes repeatedly for approximately 30 seconds. After 5 days of this daily agitation, the thick collagen solution was uniform and clear and free from visible opaque collagen masses.

2.2.2 Formation of hydrated collagen gels—Acellular collagen gels were prepared for structural and mechanical studies into collagen disks 2 mm in thickness and 8 mm in diameter using a PDMS mold. Gels with a final concentration of 3, 8, 10, 15, and 20 mg/ml were made from concentrated collagen stock solutions of 8, 10, 20, 20, and 30 mg/ml, respectively. This preparation proceeded as follows: 1) The desired mass of collagen was placed in a separate Eppendorf tube (tube 1) and kept on ice. 2) The dilutant was prepared in an Eppendorf tube (tube 2) and kept on ice. The dilutant consisted of 0.1 volume fraction (with respect to the desired final total volume of solution) of 10× concentrated Medium 199. Ice cold 1N NaOH was added to the 10× M199 (volume of 1N NaOH added = (volume of collagen in tube 1) *0.02). The dilutant was brought up to the final volume by adding 1× M199 to tube 2. 3) The basic M199/NaOH solution (tube 2) was slowly mixed on ice into the acidic collagen solution (tube 1) using a small spatula. 4a) For acellular gels, once the collagen solution was at neutral pH (determined from phenol red dye in media), neutralized collagen solution was dispensed immediately in a PDMS mold and allowed to polymerize at 37 °C at 5% CO_2 for 20 minutes. 4b) Alternatively, for scaffolds with cells in the bulk of the gel (Vasculogenesis Assay – Materials and Methods), once the collagen solution was neutralized, the appropriate volume of concentrated cell suspension (at 6×10^6 cells/ml) was mixed into the neutralized collagen solution. This mixing process required extreme care and was performed manually with a spatula to ensure an initial homogeneous distribution of cells and to prevent bubble formation and cell damage. The neutralized collagen solution (with and without embedded cells) was placed into wells and allowed to polymerize at 37 °C at 5% CO_2 for 20 minutes.

2.2.3 Fabrication of molds for gelation and microfluidic device—PDMS wells (PDMS walls, glass bottom) of 8 mm diameter were used for the acellular structural and mechanical experiments. Circular holes on a 2 mm thick PDMS slab were created with an 8 mm biopsy punch. Wells were made by placing PDMS slabs with punched 8mm holes on a clean glass slide. Collagen solution was either pipetted (3 and 8 mg/ml) or injected from a syringe (10, 15, 20 mg/ml) into the wells with a syringe.

PDMS wells (PDMS walls and bottom) of 4 mm diameter were used for the cellular assays. Soft lithography [38] was used to generate PDMS wells. Specifically, a layer of SU8-2100 was spun, exposed, and developed to generate 1 mm thick posts with diameters of 4 mm. PDMS wells were made by treating the SU8 masters with a vapor of (tridecafluoro-1,1,2,2-tetrahydrooctyl)-1-trichlorosilane overnight and then curing the PDMS on the silanized SU8 structures to form an array of PDMS wells. Excess PDMS was cured on the SU8 structures so that the SU8 posts did not form complete holes through the PDMS slab, but instead, created a well with a bottom thickness of 500 μm. The PDMS was peeled away from the SU8 master and a 6 mm biopsy punch was used to separate individual wells.

To determine the lower limit of collagen concentration that can retain microstructure, we replicated micro pores in collagen concentrations of 0.15%, 0.3%, 0.6% and 1.0%. Soft lithography [38] was used to generate a PDMS stamp as a master on which to pattern collagen with microstructure[15]. The molding proceeded in two steps, from a microfabricated positive

mold in SU-8 (wells) to a negative mold in PDMS (posts), and from this PDMS to the final structure in collagen (wells). Specifically, a layer of SU8-2100 was spun, exposed, and developed to generate 400 μm-deep pores with diameters of 50 μm. PDMS stamps were made by curing the PDMS on the silanized SU8 structures (described above) to form a PDMS stamp, a negative of the SU8 consisting of an array of PDMS pillars of 400 μm-height on one face. Finally, cylindrical wells on a separate 2 mm thick PDMS slab were created with a 4 mm biopsy punch. This PDMS slab was needed to create a well above the pillars on the PDMS stamp to contain the collagen solution before it gelled. This slab with the wells was treated with 1% poly(ethyleneimine) (PEI) solution for 10 minutes followed by 0.1% glutaraldehyde (GA) for 30 minutes. This treatment made the PDMS wells adherent to collagen.

The PDMS stamp and the PDMS wells were rinsed twice for 15 minutes with sterile water and were then washed overnight in sterile water at room temperature on a shaker. Following the wash steps, the dried PDMS slab was placed on the PDMS stamp to create wells above the PDMS pillars. Collagen of various concentrations (0.15%, 0.3%, 0.6%, 1%, and 2%) was prepared from the concentrated stock solutions and gelled in the wells of the PDMS stamp by incubating at 37 °C with 5% CO_2 for 30 minutes as described above in the formation of hydrated collagen gels section. Because the collagen adhered to the PEI/GA coated PDMS wells, the molded collagen could be peeled away from the PDMS stamp by handling only the PDMS wells and without direct handling of the collagen gel. Gels were then imaged on a Nikon Eclipse TS100 microscope with an Olympus DP70 Camera using DP Controller software.

Microfluidic collagen was fabricated in a manner similar to our previous approach presented in Choi, et al. [15]: 1) uncross-linked collagen was injected into a closed mold where a micropatterned PDMS stamp was inserted, and 2) cross-linked collagen with an imprinted microfluidic network was then pressure-sealed against a 1.2 mm-thick glass slide (Ted Pella, Inc., Redding, California) as illustrated in Fig. 5. Functionality of microfluidic collagen was examined by delivering RITC-dextran (MW 70 kDa) in PBS via microchannels at a flow rate of 10 uL/min (Fig. 5c).

2.2.4 Fluorescently labeling collagen fibers—To visualize collagen fibers with confocal fluorescence microscopy and to analyze a collagen gel's structural properties, tetramethylrhodamine isothiocyanate (TRITC)-labeled collagen was prepared by reacting pure collagen with TRITC following a standard labeling protocol [39]. Specifically, dry collagen was resuspended at 20 mg/ml in 0.1M sodium bicarbonate buffer at pH 9.0 by agitating for 8 hours at 4°C. A 10mg/ml TRITC solution in DMSO was added to the collagen at a molar ratio of 3:1, dye: protein [39] and was then agitated at 4°C for 24 hours in the dark. Free dye molecules were removed using dialysis in 0.1% acetic acid for at least 72 hours in the dark at 4°C using dialysis tubing with a molecular weight cut off of 25,000 Da. The labeled collagen was kept at 4°C in the dark until used.

2.2.5 Structural analysis—Both confocal fluorescence and reflectance microscopy of the TRITC-labeled collagen were performed on unfixed, hydrated samples (Fig.1). Confocal reflectance microcopy requires no staining and collects the back-scattered light from the collagen fibers [40]. We used our fluorescently labeled collagen fibers [39] to directly compare the resolution of the two visualization methods, and we collected the reflected light and the fluorescence channel simultaneously on the same sample (Fig. 1a and b). Line scans across the same fibers in the reflectance and fluorescence images were performed and the full width at half maximum (fwhm) was determined by fitting to a Gaussian distribution (Fig. 2d). Line scans across single fibers were performed to determine and average fiber diameter (Fig.3) for each collagen concentration.

2.3 Mechanical consideration

2.3.1 Mechanical properties of dense collagen scaffolds—We used confined compression to characterize the mechanical properties of collagen gels[24]. Transient compression-stress relaxation experiments were performed on hydrated acellular collagen gels. By submerging the entire PDMS mold in phosphate buffered saline (PBS) and peeling the PDMS free from the collagen, gels simply floated off the mold into PBS without direct physical contact to the collagen. Because the low concentration collagen gels are extremely fragile and can collapse upon touching, gentle handling of the collagen discs was crucial to maintain the integrity of the gels. Gels were mechanically tested within 24 hours of polymerization.

The compression-stress relaxation experiments were done with an Enduratec ELF-3200 test system (Bose EnduraTEC, Minnetonka,MN) using a 250-g load cell (Honeywell Sensotec, Columbus, OH). Briefly, the collagen discs were placed in an impermeable cup with the same dimensions as the sample. A polyethylene porous plug was placed on the submerged sample, and the displacement actuator was brought into contact with the porous plug. Due to the confinement provided by the cup, as load was applied to the sample, liquid could only exit the gel through the porous plug. Since the liquid could penetrate the porous plug but the gel could not, there was relative motion between the two phases. Gels were compressed in increments of strain, $\Delta\varepsilon$= 3% strain up to 30% strain. After each increment, the sample thickness was held constant for 20 minutes to allow the stress to relax toward a new equilibrium.

2.3.2 Mechanical model—Using a custom MATLAB (The Mathworks, Natick, MA) code developed by the Bonassar Lab at Cornell[41], stress relaxation data was fit to a poroelastic model of material behavior using the equation:

$$\sigma_{eq}=A\left(1-e^{-t/\tau}\right)+B \quad [1]$$

where σ_{eq} [Pa] is the instantaneous stress, B [Pa] is the equilibrium stress, t [s] is time, and τ [s] is the exponential time constant[41]. We make the assumption, following others [42], that the gel matrix responds like an isotropic, elastic material. The transient stress relaxation and final equilibrium stress data were recorded and an equilibrium stress-strain curve was generated for each sample.

The longitudinal equilibrium modulus, M_{eq} [Pa] was calculated from the slope of the curve of equilibrium stress vs. strain: σ_{eq} vs. ε. Note that the longitudinal modulus is related to the Young's modulus, E, and the Poisson's ratio, ν by the following expression:

$$M_{eq}=E\frac{1-\nu}{(1+\nu)(1-2\nu)} \quad [2]$$

The Poisson ratio was been estimated to be 0.2 for collagen networks[43]. On very short time scales the gel is essentially incompressible ($\nu\cong0.5$), but on a longer time scale which is relevant for the confined compression test, the gel appears compressible ($0<\nu<0.5$). Given this assumption, E = 0.9*M. The transient relaxation data was used to calculate the hydraulic permeability, k [m^2/Pa*s]:

$$k=\frac{\delta^2}{\pi^2 * \mathrm{M}_{eq} * \tau} \quad [3]$$

where δ [*m*] is the thickness of the sample[42]. Three to five collagen discs were tested for each collagen concentration. Each sample was compressed to 30% strain only once. A summary of the mechanical testing results can be found in Fig. 5.

2.3.3 Calculation of hydraulic radius—The confined compression testing allowed us to measure the hydraulic permeability, k [cm^2] via Eq. 3 (Fig. 4b). We used the Carman-Kozeny equation to relate k to the mean hydraulic radius, r_H [m](reported in Table 1), as described in [44]. The Carman-Kozeny model treats the gel as an array of cylinders (which were fibers in our case) assumed to be randomly oriented in 3-D. It predicts the following relationship:

$$k=\varepsilon * r_H^2 / k_{geo} \quad [4]$$

where k_{geo} is a geometric factor which depends on the tortuosity and ε is effective porosity defined as:

$$\varepsilon=(1-\phi) \quad [5]$$

In Eq. 5, ϕ is the product of the collagen concentration and the effective specific volume of collagen (protein + bound water), previously reported at 1.89 mg/g [45].

The geometric factor is separated into its parallel and normal components with respect to flow coordinates. For cylinders (fibers) perpendicular to the flow,

$$k_{\|}=2\varepsilon^3 / \left\{(1-\varepsilon)*\lfloor 2*\ln\left(1/1-\varepsilon\right)-3+4*(1-\varepsilon)-(1-\varepsilon)^2\rfloor\right\} \quad [6]$$

and for cylinders parallel to the flow,

$$k_{\perp}=2\varepsilon^3 / \left\{(1-\varepsilon)*\lfloor \ln\left(1/1-\varepsilon\right)-(1-(1-\varepsilon))^2/\left(1+(1-\varepsilon)^2\right)\rfloor\right\} \quad [7]$$

For cylinders oriented randomly in 3-D the geometric factor is given by,

$$k_{geo}=(2k_{\perp}+k_{\|}) \quad [8]$$

In evaluating Eqs. 6–8 for k_{geo} (Table 1), Eq. 5 and the effective specific volume of collagen was used to calculate the porosity.

2.4 Biological characterization

2.4.1 Cell culture—Human umbilical vein endothelial cells (HUVECs) were used in passages 3–10. Cells were cultured in growth media, and this growth media was changed every 2–3 days. Oral squamous cell carcinoma (OSCC-3) cells (a gift from Peter Polverini, University of Michigan) were cultured as described previously[46].

2.4.2 Vasculogenesis Assay—To set up the vasculogenesis assays, cells at 75–95% confluency were washed with HEPES buffered saline solution, removed from culture flasks with trypsin-EDTA, neutralized with growth media, centrifuged, and resuspended at 6×10^6 cells/ml. Cell-seeded collagen gels were prepared from a concentrated, acidic stock collagen

solution. Cell-seeded gels were either pipetted (for 3mg/ml and 8mg/ml collagen concentrations) or injected with a 250 μl syringe into 4 mm diameter PDMS wells that were set, one per well, in 48-well plates and were allowed to gel at 37°C and 5% CO_2 for 30 minutes. A volume of gel was used so that the top surface was approximately flush with the top of the wells. 300 μl of vasculogenesis media was added to each well in the 48-well plate. Vasculogenesis assays were kept at 37°C and 5% CO_2 for 3, 7, 14, or 21 days before fixing and staining. Cultures were re-fed with the above assay media every 48–72 hours.

2.4.3 Invasion Assay—To set up the invasion assays, collagen gels were prepared from concentrated stock solutions as described above and either pipetted (for 3mg/ml and 8mg/ml collagen concentrations) or injected with a 250 μl syringe into 4 mm diameter PDMS wells that were set, one per well, in 48-well plates and were allowed to gel at 37°C and 5% CO_2 for 30 minutes. HUVECs (200cells/mm^2) were then seeded on top of the gel and allowed to attach for 30 minutes before placing 300 μl vasculogenesis media into the wells.

2.4.4 Co-culture—Similar to the vasculogenesis assays described above, oral squamous cell carcinoma (OSCC-3) cells were seeded in 6.75 mg/ml collagen gels at a concentration of 2×10^7 cells/ml into molded into PDMS wells and allowed to gel at 37°C and 5% CO_2 for 30 minutes. OSCC-3-containing gels were then top-seeded with HUVECs at a density of 300 cells/mm^2. Co-cultures were maintained for 3 days the HUVEC growth media, supplemented with 50ug/ml L-ascorbic acid and 50 ng/ml TPA.

2.4.5 Staining and Microscopy—At the designated time points during the invasion and vasculogenesis assays and co-culture experiment, gels and cells were fixed and stained with a 1:100 dilution of Alexa Fluor 488 phalloidin or Alexa Fluor 568 phalloidin and 1:1000 dilution of 4',6-diamidino-2-phenylindole (DAPI) (ex 368/em 461) or YOYO-1 iodide (ex 491/ em 509). For the co-culture experiment endothelial cells were also stained with CD-31 mouse anti-human/AlexaFluor 488 goat anti-mouse. With the exception of the permeabilization step, all incubations were conducted at room temperature with agitation. Permeabilization was performed at room temperature without agitation.

Confocal images of the invasion and vasculogenesis assays and co-culture experiments were obtained using a Zeiss 510 Meta confocal microscope (Zeiss, Welwyn Garden City, United Kingdom) with a 63×, NA 1.4 oil immersion objective, a 40×, NA 1.3 oil immersion objective, or a 40×, NA 1.2 water immersion objective with a pinhole of one Airy Unit. Image stacks were accumulated with a z-step between each successive optical slice of 2 to 4 μm. Cross sections of the z-stack were rendered in the Zeiss Image Browser.

3 Results and Discussion

3.1 Fiber structure in gels

Cells sense and respond to their physical and chemical surroundings; thus, when cells are embedded in a 3-D environment, the fiber structure and density significantly influence cellular morphology, behavior, and phenotype. We analyzed the fiber density and fiber diameter of collagen matrices to characterize the local cellular environment. The structure of these dense collagen matrices was a complicated, intertwined meshwork of fibers. The confocal images in Fig. 1 (b–f) revealed increasing spatial density of fibers as collagen concentration increased from 3mg/ml to 20 mg/ml which was expected based on previous reports [47]. As depicted in Fig. 2 (a–c), fiber diameter appeared relatively constant even as collagen concentration increased.

Confocal reflectance is commonly used to visualize collagen fibers because it is simple, requiring no chemical processing or staining; however, we found that confocal fluorescence

imaging of TRITC-labeled collagen fibers produced higher resolution and images. The fluorescence images showed better resolution as demonstrated by the full width at half maximum (fwhm) of the Gaussian fits of peaks in line scans across a single fiber in each type of image (Fig. 2(d)). Line scans were performed at the identical location of the reflectance (Fig. 1(a)) and fluorescent (Fig. 1(b)) images. In addition, the fluorescent images showed better sensitivity than reflectance as a line scan across a series of four fibers (Fig. 2(e)) showed more visible fibers present in the fluorescent image. This imaging method comparison provides a basis for interpreting reflectance images in the future.

Based on line scans perpendicular to single fibers, the average fiber diameter in well-mixed collagen gels at all concentrations was ~ 500 μm (Fig. 3), in good agreement with previously reported values[48]. This constant fiber diameter indicates that the increase in the modulus with increasing concentration collagen (Fig. 4) likely resulted from the increase in fiber entanglement rather than from the properties of the individual fibers [24,48].

At high collagen concentration (20 mg/ml), a larger range of diameters appeared (Fig. 3). We have determined that if the high concentration collagen (1.5% or 2.0%) was inadequately mixed or if the lyophilized collagen had not been completely dissolved (<5 days in acetic acid) (Fig. 3 inset) the fiber size was inhomogeneous and large fibers existed. Using single plane confocal fluorescent images (as in Fig. 1b–f), we also calculated the average pore radius for each collagen concentration. We found that the pore radius ranged from ~1 μm (0.3%) to ~15μm (2.0 %) (Table 1).

3.2 Mechanical consideration

It is well established that the specific mechanical properties of the cellular microenvironment influence cell behaviors[7]. Similarly, the degree to which the ECM can transduce force and deformation at the microscale directs cell growth [49], differentiation [50] and tissue formation [51]. We investigated the mechanical characteristics of the collagen matrices to understand better the biomechanics of the material and its role in cell and tissue dynamics. Fig. 4 presents the modulus and permeability results obtained from stress-relaxation experiments using confined compression testing. The equilibrium modulus, M_{eq} increased significantly as collagen concentration increased from 0.3% to 2.0% from ~30 Pa to ~1800 Pa (Fig. 4a).

These mechanical measurements provide a comparison to previous values measured for collagen gels and to native tissue measurements. Our values for the 0.3% collagen matrices are in good agreement with previously reported values for self-assembled collagen matrices [24]. To our knowledge, modulus values for the higher concentration gels have not been reported in the literature. Tissues *in vivo* exhibit a large range of stiffnesses depending on the type of tissue (e.g. elastic modulus of brain tissue ranges from 0.1–1 kPa and of muscle ranges from ~8–17 kPa [52]. Pathological tissues, like tumors have been shown to contain a dense collagen matrix with concentrations of 1– 4% [26]. The elastic modulus of four types of tumor ranges from 0.66 to 39 kPa [53]. Our 1.0% (0.6 kPa), 1.5% (1.0 kPa), and 2.0% (1.8 kPa) collagen matrices fall within the range for brain tissue and tumors.

The hydraulic permeability, extracted from the relaxation time constant (Eq. 3), decreased exponentially with collagen concentration over three decades (Fig. 4b). A decrease was expected as researchers have shown that hydraulic permeability is inversely correlated to collagen content both *in vivo*[54] and *in vitro*[26]. Others have extracted the hydraulic permeability of type I collagen gels from confined compression data and report a permeability value of 2×10^{-9}cm^2 for 0.3% collagen gels[24], to be compared to 3×10^{-7}cm^2 in our measurements. Ramanujan et al. have measured the Darcy permeability of 1.0% collagen matrices and report a value of ~1×10^{-11} cm^2 [26], to be compared to 7.5×10^{-9}cm^2 in our measurements. These previously reported values are significantly lower than our reported

values. A potential source of this inconsistency is differences in methodologies. For example, we use a step deformation while others have used creep tests [24]. It is likely that the collagen matrices have both a solid viscoelastic component and a poroelastic component to the mechanical response. The higher strain rate in a step deformation (as compared to creep) would produce a large, quickly decaying viscous stress which could modify the poroelastic relaxation that we used to calculate the hydraulic permeability.

Another possible source for the inconsistency in permeability values is that the materials between research groups simply have significantly different microstructure. For instance, there is a discrepancy between in the microstructure of our matrix (Fig. 1b and Table 1) and the interfibrillar spacing of 1 μm estimated with a creeping flow analysis in [24]. Similarly, the higher mass fraction gels created by Ramanujan et al.[26] were obtained via centrifugation, possibly altering the tortuosity and microstructure of the network.

Using the hydraulic permeability values from Fig. 4b and the Carmen-Kozeny equation (Eq. 4), we estimated a hydraulic radius, r_H, for each collagen concentration and compared it to our 2-D image analysis pore radius measurements (Table 1). We note that the two measures of structure (r_H and a) agree well except for the two lowest mass fractions (Table 1). This agreement at higher mass fractions ($\geq$ 10 mg/mL), suggests that our methods are appropriate in this range. At the lowest mass fractions (0.3% and 0.8%), the hydraulic values, r_H, are much larger than those extracted by image analysis from 2-D sections. As noted above, the discrepancy at low mass fractions could be caused by a large viscous term induced by the step deformation method. Other potential sources of the low mass fraction discrepancies include: 1) deformation of the pore structures by the perfusion flow; this effect would be more pronounced at low volume fractions for which the modulus of the network was observed to be lower (Fig. 4a), and 2) inaccuracy of evaluation by of pore size in 2-D sections. Extracting quantitative measurements of pore size based on a 2-D plane of a 3D filamentous network is not trivial . Our method of extracting pore size by analyzing the nearest points on collagen fibers in sections of confocal image stacks could explain the factor of 10 difference in the estimated radius.

3.3 Microfabrication and microfluidics

Microfluidic control within a 3-D cell remodelable hydrogel is a desirable tool for cell biologist and tissue engineers. A robust microfluidic biomaterial in type I collagen would allow scientists to engineer spatially complex tissues as it would give them control over 1) the delivery of oxygen and nutrients into the bulk, 2) the temporal presentation of specific factors to cells in a 3-D environment, and 3) microvascular luminal flow and shear stresses[55]. Here we tested and determined the lower bound on collagen concentration necessary for both the molding of simple pores and microfluidic structures. We tested both the simple pores and microfluidic structures as some simple experiments may only require a micropore within a biomaterial rather than a functional microfluidic channel.

We have molded circular pores with a diameter of 50 μm into collagen matrices with mass fractions of (0.15%, 0.3%, 0.8%, and 1.0%). For mass fractions of 0.3% or greater, the reproduction was clean and reproducible (Fig. 5a). At 0.15%, however, circular pores could not be reproducibly molded. Frequently pores molded in 0.15% collagen would become deformed during the release process and would collapse (data not shown). Thus, we conclude that the lower bound for fabrication of this simple pore structure was 0.3%.

Using a custom molding jig (Fig. 5b), microfluidic devices were fabricated in 1.0%, 1.5% and 2.0% collagen concentrations and maintained flow (1 μL/min) and sterility in a cell culture incubator without leaking for over three weeks. We verified that sterile conditions were maintained by collecting and analyzing the output media. Note that the device was pressure

sealed to glass leaving a 3-sided collagen channel (Fig. 5b). A device using 0.6% collagen was attempted and failed. Specifically, only a portion of the microfluidic network formed a seal with the bottom glass slide. Flow was introduced at 1 μL/min which resulted in a flow speed of ~ 1 mm/s. There was significant leakage at the inlet and outlet and after 15 minutes of flow, the initially sealed portion of the network began to leak. The modulus of the 0.6% collagen is low enough that the gel deforms and collapses easily during device assembly and even just by the perfusion flow. Thus, we conclude 1.0% collagen was the lower bound to create a functional microfluidic device (Fig. 5c).

The development of scaffolds with embedded microfluidic structure provides one context in which the hydraulic permeability of the matrix is important. As pointed out by Choi et al., the delivery of solutes via embedded microchannels is simplified if the hydraulic permeability of the matrix is low compared to that of the microchannels[15]. The alginate had a low hydraulic permeability (3×10^{-10} cm^2[56]) as compared to the convective permeability through the embedded microchannels; therefore, the mass transfer from the channels into the gel was dominated by diffusion. In the same manner, to use type I collagen as a microfluidic biomaterial, the hydraulic permeability within the bulk material must be sufficiently small compared to the permeability through the embedded microchannels. We verified this condition by comparing the hydraulic permeance of the matrix, p_m [m·s] to the hydraulic permeance of the microchannel, p_c [m·s] [56]. We define the hydraulic permeance of the matrix as

$$p_m = k\left(\frac{A}{L}\right)\left(\frac{\rho}{\mu}\right) \quad [9]$$

where k [m^2] is permeability of the matrix, A [m^2] is interfacial cross-sectional area between a microchannel and the matrix, L [m] is length of the microchannel, ρ [kg/m^3] is density of fluid, and μ [Pa·s] is viscosity of fluid. Similarly, we define hydraulic permeance of the microchannel, p_c [m·s] as

$$p_c = \frac{\pi d_h^4 \rho}{128 \mu L} \quad [10]$$

where d_h [m] is hydraulic diameter of the microchannel [57]. Note that the direction of convective flow in the microchannel is parallel to that of permeation to the matrix, and we consider a simplified block of microfluidic collagen with L = 1.5 mm, $w_c = h_c = d_h$ = 100 μm, $k = 10^{-8}$ cm^2, $A = 3(h_c L)$, $p_m = 3.4\times10^{-8}$m·s and $p_c = 1.8\times10^{-7}$m·s. We calculate an effective permeability of the 1.0% collagen matrix of $0.18p_c$. Indeed, the effective permeabilities of the high weight percent collagen gels (1.0%, 1.5%, and 2.0%) are sufficiently low such that convective mass transfer is contained largely within the microchannels and diffusive mass transport should dominate the delivery of solutes to the bulk material.

3.4 Remodeling of dense collagen by ECs

We determined the variations in the rate and extent of remolding, vasculogenesis, and invasion by ECs as a function of the concentration of collagen (Fig. 6 and Fig. 7). Three-dimensional (3-D) vasculogenesis assays have been used to identify and characterize angiogenic promoters and inhibitors and to study capillary tube formation[21]; however, tube formation and invasion within dense collagen (>1%) have not been studied.

3.4.1 Tube formation—Using confocal reflectance microscopy, we observed that endothelial cells seeded into the bulk of the gels created circular voids in the collagen[35] at

all concentrations by 21 days (Fig. 6). The circular voids are lined by endothelial cells, and we interpret them as cross-sections of tubes. The voids may be areas of collagen degradation or areas where cells pushed the collagen out of the way. In either case, cells had remodeled (either degraded or displaced) the collagen at earlier time points (3 days) for all collagen concentrations; however, in general, the extent of remodeling increased with time and decreased with collagen concentration. We note that there were differences in the collagen structure around the voids (lighter regions as compared to the bulk) at 3 days for the 0.3% collagen gels and at 21 days for all collagen concentrations (Fig. 6, arrow in t=21 of 0.3% gels). Lighter regions were more prevalent and extended further around the collagen voids in lower mass fraction gels (0.3, 0.6, and 1.0%). These light areas could be 1) denser regions of collagen that has been pulled or gathered in towards the cells, 2) matrix deposited by the endothelial cells, or 3) stronger scattering of light due to changes in the alignment or diameter of fibers .

3.4.2 Network formation—After staining the f-actin network and the nuclei of the endothelial cells, we used confocal fluorescence microscopy to visualize the cellular structures within dense collagen matrices. We saw visible lumen formation in the *xy* plane at all collagen concentrations by day 3 (Fig. 7a). We captured a *z*-stack of images at each concentration and time point and generated *xz* planes to visualize the extent of network formation from the boundary into the bulk (Fig. 7c,d). A 3-D connected network (an open, continuous tube that was supported from the bottom stiff boundary in the *z*-direction) with many connections emerged in the 0.3% collagen at 3 days, in the 0.8 % at 7 days, and in the 1.0% collagen at 21 days (Fig. 7c,d).

We quantified lumen area and frequency for the different collagen concentrations over time (Fig. 8a,b). In general, lumen density and area both increased with time. Lumen density and area both decreased with an increasing collagen concentration, likely due to the increase in steric hindrance with an increase of concentration. At the low mass fractions, lumen frequency decreased slightly from day 3 to day 7 (Fig. 8b), possibly due to tube regression; however, this decrease was not statistically significant.

3.4.3 Angiogenic invasion—HUVEC invasion experiments are commonly used to study the development of capillary sprouts and tubes[21]. These types of experiments typically monitor the invasion of endothelial cell into low weight percent collagen gels (usually ~0.25%) over the course of about 2–3 days. We performed similar invasion experiments but used collagen concentrations up to 20 mg/ml. Based on the collagen structure and pore size at higher concentrations (Fig. 1), the dense collagen presumably provided significantly more steric hindrance for cells, so we allowed the invasion assays to culture for up to three weeks.

HUVECs formed a monolayer on top of collagen, and cells invaded over time (Fig. 9). As expected, invasion distance and frequency decreased with increasing collagen concentration (Fig. 10) at early times. We saw very little invasion in 2% collagen even after 21 days of culture (arrow in Fig. 9 points to a cell structure that has invaded ~ 20 μm). We found that invasion distance steadily increased during the first 14 days of culture for 0.3, 0.6 and 1% collagen gels (Fig. 10a). Invasion distance continued to increase for the 0.6% and 1% collagen gels until day 21; however, did not continue to increase in the 0.3% gels. The invasion frequency grew monotonically out to ~ 7 days in the 0.3% collagen and out to day 21 for the higher concentration collagen matrices (Fig. 10b).

Note that significant tube regression in 0.25% collagen gels has been reported[58] which is consistent with our observation of an absence of further invasion in the 0.3% gels. This observation points to an advantage of higher mass fractions for the development of functional vascular structure. At early times, the length of the invasions scaled like 1/[Collagen] (invasions in 0.6% are half as long as in 0.3% and so on). This observation is compatible with the

hypothesis that degradation is the rate limiting step during the invasion process [35]. Finally, vasculogenic activity (Fig. 7) was much less heavily suppressed by increasing mass fraction than invasion (Fig. 9) suggesting a fundamental difference in cell behavior and activity when endothelial cells were seeded in a 3-D (vasculogenesis assay) versus 2-D (invasion assay) format.

3.5 Co-culture of ECs and cancer cells

Tumor growth depends on the cancer cell's ability to promote angiogenesis by the expression of pro-angiogenic proteins such as VEGF, bFGF, and IL-8 [10]. To mimic tumor-cell-initiated angiogenesis *in vitro*, we developed a model that consisted of a 3-D co-culture of oral squamous cell carcinoma (OSCC-3) cells in the bulk of a high mass fraction collagen gels and HUVECs seeded on the matrix surface. HUVECs formed a confluent monolayer (Fig. 11), and tumor cells survived and proliferated (measured by DNA assay- data not shown) while embedded within the dense collagen matrix (solid arrow in Fig. 11). Endothelial cells invaded towards the OSCC-3 cells into the bulk of the collagen gel when co-cultures were maintained for more than 3 days (open arrows in Fig. 11). Others have demonstrated that OSCCs secrete IL8 and VEGF in 3-D these type of cultures[46], thus, this invasion was likely initiated by the secretion of pro-angiogenic factors possibly due to hypoxic conditions within the dense collagen matrix. Further studies using this model of tumor angiogenesis *in vitro* could advance the development of cancer anti-angiogenic therapies.

4 Conclusions

We have demonstrated that dense collagen matrices are mechanically robust while they maintain the ability to be remodeled by tissue cells. We have identified a window of collagen concentrations (>10mg/ml and <20 mg/ml) that is above the lower bound for microfabrication and below the upper bound for cellular remodeling. Because dense collagen can be supportfunctional microstructure and be remodeled by cells, there is potential to control the spatial and temporal chemistry and hydraulic stresses experienced by endothelial cells and cells in the bulk within these scaffolds. Endothelialized microfluidic collagen scaffolds would provide a basis for an advanced *in vitro* tumor model that mimics conditions *in vivo* including ECM density and a vascular network with flow adjacent to a model solid tumor [59]. Such a model has the potential to be used as an *in vitro* platform for tumor metastasis and angiogenesis studies or leukocyte extravasation and intravasation. In addition to an *in vitro* model, our microfabricated dense collagen matrices could be valuable as a pre-vascularized tissue engineered, implantable scaffold.

Acknowledgments

We acknowledge Glenn Swan, Mingming Wu, and George Davis for their support. We acknowledge funding from the Cornell Nanobiotechnology Center (supported by the STC Program of the National Science Foundation under Agreement No. ECS-9876771), the Beckman Foundation, NYSTAR, the Morgan Fund for Tissue Engineering, the NIH (RC1 CA146065, 1U54 CA143876-01) and the Cornell Center for Nanoscale Science (Grant ECS 03-35765).

References

1. Langer R, Vacanti JP. Tissue engineering. Science 1993;260:920–926. [PubMed: 8493529]
2. Pedersen JA, Swartz MA. Mechanobiology in the third dimension. Ann Biomed Eng 2005;33:1469–1490. [PubMed: 16341917]
3. Nelson CM, Vanduijn MM, Inman JL, Fletcher DA, Bissell MJ. Tissue geometry determines sites of mammary branching morphogenesis in organotypic cultures. Science 2006;314:298–300. [PubMed: 17038622]

4. Fidler IJ. Critical factors in the biology of human cancer metastasis: twenty-eighth G.H.A. Clowes memorial award lecture. Cancer Res 1990;50:6130–6138. [PubMed: 1698118]
5. Ferrara N. VEGF and the quest for tumour angiogenesis factors. Nat Rev Cancer 2002;2:795–803. [PubMed: 12360282]
6. Levenberg S, Rouwkema J, Macdonald M, Garfein ES, Kohane DS, Darland DC, et al. Engineering vascularized skeletal muscle tissue. Nat Biotechnol 2005;23:879–884. [PubMed: 15965465]
7. Discher DE, Janmey P, Wang YL. Tissue cells feel and respond to the stiffness of their substrate. Science 2005;310:1139–1143. [PubMed: 16293750]
8. Sieminski AL, Hebbel RP, Gooch KJ. The relative magnitudes of endothelial force generation and matrix stiffness modulate capillary morphogenesis in vitro. Exp Cell Res 2004;297:574–584. [PubMed: 15212957]
9. Reinhart-King CA, Dembo M, Hammer DA. Cell-cell mechanical communication through compliant substrates. Biophys J 2008;95:6044–6051. [PubMed: 18775964]
10. Fischbach C, Kong HJ, Hsiong SX, Evangelista MB, Yuen W, Mooney DJ. Cancer cell angiogenic capability is regulated by 3D culture and integrin engagement. Proc Natl Acad Sci U S A 2009;106:399–404. [PubMed: 19126683]
11. Anseth KS, Bowman CN, Brannon-Peppas L. Mechanical properties of hydrogels and their experimental determination. Biomaterials 1996;17:1647–1657. [PubMed: 8866026]
12. Jo S, Shin H, Mikos AG. Modification of oligo(poly(ethylene glycol) fumarate) macromer with a GRGD peptide for the preparation of functionalized polymer networks. Biomacromolecules 2001;2:255–261. [PubMed: 11749181]
13. Kloxin AM, Kasko AM, Salinas CN, Anseth KS. Photodegradable hydrogels for dynamic tuning of physical and chemical properties. Science 2009;324:59–63. [PubMed: 19342581]
14. Lutolf MP, Hubbell JA. Synthetic biomaterials as instructive extracellular microenvironments for morphogenesis in tissue engineering. Nat Biotechnol 2005;23:47–55. [PubMed: 15637621]
15. Choi NW, Cabodi M, Held B, Gleghorn JP, Bonassar LJ, Stroock AD. Microfluidic scaffolds for tissue engineering. Nat Mater 2007;6:908–915. [PubMed: 17906630]
16. Williams BR, Gelman RA, Poppke DC, Piez KA. Collagen fibril formation- optimal in vitro conditions and preliminary kinetic results. J Biol Chem 1978;253:6578–6585. [PubMed: 28330]
17. Elsdale T, Bard J. Collagen substrata for studies on cell behavior. J Cell Biol 1972;54:626–637. [PubMed: 4339818]
18. Folkman J, Haudenschild C. Angiogenesis in vitro. Nature 1980;288:551–556. [PubMed: 6160403]
19. Ceballos D, Navarro X, Dubey N, Wendelschafer-Crabb G, Kennedy WR, Tranquillo RT. Magnetically aligned collagen gel filling a collagen nerve guide improves peripheral nerve regeneration. Exp Neurol 1999;158:290–300. [PubMed: 10415137]
20. Eschenhagen T, Fink C, Remmers U, Scholz H, Wattchow J, Weil J, et al. Three-dimensional reconstitution of embryonic cardiomyocytes in a collagen matrix: a new heart muscle model system. FASEB J 1997;11:683–694. [PubMed: 9240969]
21. Davis GE, Black SM, Bayless KJ. Capillary morphogenesis during human endothelial cell invasion of three-dimensional collagen matrices. In Vitro Cell Dev Biol Anim 2000;36:513–519. [PubMed: 11149750]
22. Bell E, Ivarsson B, Merrill C. Production of a tissue-like structure by contraction of collagen lattices by human fibroblasts of different proliferative potential in vitro. Proc Natl Acad Sci U S A 1979;76:1274–1278. [PubMed: 286310]
23. Mueller-Klieser W. Tumor biology and experimental therapeutics. Crit Rev Oncol Hematol 2000;36:123–139. [PubMed: 11033302]
24. Knapp DMBV, Moon AG, Yoo K, Petzold LR, Tranquillo RT. Rheology of reconstituted type I collagen gel in confined compression. J. Rheol 1997;41:971–993.
25. Vernon RB, Sage EH. Contraction of fibrillar type I collagen by endothelial cells: a study in vitro. J Cell Biochem 1996;60:185–197. [PubMed: 8655629]
26. Ramanujan S, Pluen A, McKee TD, Brown EB, Boucher Y, Jain RK. Diffusion and convection in collagen gels: implications for transport in the tumor interstitium. Biophys J 2002;83:1650–1660. [PubMed: 12202388]

27. Tien J, Nelson CM, Chen CS. Fabrication of aligned microstructures with a single elastomeric stamp. Proc Natl Acad Sci U S A 2002;99:1758–1762. [PubMed: 11842197]
28. Chrobak KM, Potter DR, Tien J. Formation of perfused, functional microvascular tubes in vitro. Microvasc Res 2006;71:185–196. [PubMed: 16600313]
29. Golden AP, Tien J. Fabrication of microfluidic hydrogels using molded gelatin as a sacrificial element. Lab Chip 2007;7:720–725. [PubMed: 17538713]
30. Yannas IV, Burke JF. Design of an artificial skin- basic design principles. J Biomed Mater Res 1980;14:65–81. [PubMed: 6987234]
31. Lee CR, Grodzinsky AJ, Spector M. The effects of cross-linking of collagen-glycosaminoglycan scaffolds on compressive stiffness, chondrocyte-mediated contraction, proliferation and biosynthesis. Biomaterials 2001;22:3145–3154. [PubMed: 11603587]
32. Vernon RB, Gooden MD, Lara SL, Wight TN. Native fibrillar collagen membranes of micron-scale and submicron thicknesses for cell support and perfusion. Biomaterials 2005;26:1109–1117. [PubMed: 15451630]
33. Goo HC, Hwang YS, Choi YR, Cho HN, Suh H. Development of collagenase-resistant collagen and its interaction with adult human dermal fibroblasts. Biomaterials 2003;24:5099–5113. [PubMed: 14568426]
34. Helary C, Ovtracht L, Coulomb B, Godeau G, Giraud-Guille MM. Dense fibrillar collagen matrices: a model to study myofibroblast behaviour during wound healing. Biomaterials 2006;27:4443–4452. [PubMed: 16678257]
35. Davis GE, Senger DR. Endothelial extracellular matrix: biosynthesis, remodeling, and functions during vascular morphogenesis and neovessel stabilization. Circ Res 2005;97:1093–1107. [PubMed: 16306453]
36. Fischbach C, Chen R, Matsumoto T, Schmelzle T, Brugge JS, Polverini PJ, et al. Engineering tumors with 3D scaffolds. Nat Methods 2007;4:855–860. [PubMed: 17767164]
37. Bornstein MB. Reconstituted rattail collagen used as substrate for tissue cultures on coverslips in maximow slides and roller tubes. Lab Invest 1958;7:134–137. [PubMed: 13540204]
38. Whitesides GM, Ostuni E, Takayama S, Jiang X, Ingber DE. Soft lithography in biology and biochemistry. Annu Rev Biomed Eng 2001;3:335–373. [PubMed: 11447067]
39. Hermanson, G. Bioconjugate techniques. San Diego, CA: Elsevier Science; 1996.
40. Brightman AO, Rajwa BP, Sturgis JE, McCallister ME, Robinson JP, Voytik-Harbin SL. Time-lapse confocal reflection microscopy of collagen fibrillogenesis and extracellular matrix assembly in vitro. Biopolymers 2000;54:222–234. [PubMed: 10861383]
41. Roy R, Boskey A, Bonassar LJ. Processing of type I collagen gels using nonenzymatic glycation. J Biomed Mater Res A. 2009
42. Quinn TM, Grodzinsky AJ. Longitudinal modulus and hydraulic permeability of poly(methacrylic acid) gels - effects of charge-density and solvent content. Macromolecules 1993;26:4332–4338.
43. Barocas VH, Tranquillo RT. An anisotropic biphasic theory of tissue-equivalent mechanics: the interplay among cell traction, fibrillar network deformation, fibril alignment, and cell contact guidance. J Biomech Eng 1997;119:137–145. [PubMed: 9168388]
44. Pluen A, Netti PA, Jain RK, Berk DA. Diffusion of macromolecules in agarose gels: comparison of linear and globular configurations. Biophys J 1999;77:542–552. [PubMed: 10388779]
45. Levick JR. Flow through interstitium and other fibrous matrices. Q J Exp Physiol 1987;72:409–437. [PubMed: 3321140]
46. Verbridge SS, Choi NW, Zheng Y, Brooks DJ, Stroock AD, Fischbach C. Oxygen-controlled three-dimensional cultures to analyze tumor angiogenesis. Tissue Eng Part A 2010;16:2133–2141. [PubMed: 20214469]
47. Kuntz RM, Saltzman WM. Neutrophil motility in extracellular matrix gels: mesh size and adhesion affect speed of migration. Biophys J 1997;72:1472–1480. [PubMed: 9138592]
48. Roeder BA, Kokini K, Sturgis JE, Robinson JP, Voytik-Harbin SL. Tensile mechanical properties of three-dimensional type I collagen extracellular matrices with varied microstructure. J Biomech Eng 2002;124:214–222. [PubMed: 12002131]

49. Nakagawa S, Pawelek P, Grinnell F. Extracellular matrix organization modulates fibroblast growth and growth factor responsiveness. Exp Cell Res 1989;182:572–582. [PubMed: 2721593]
50. Engler AJ, Sweeney HL, Discher DE, Schwarzbauer JE. Extracellular matrix elasticity directs stem cell differentiation. J Musculoskelet Neuronal Interact 2007;7:335. [PubMed: 18094500]
51. Oster GF, Murray JD, Harris AK. Mechanical aspects of mesenchymal morphogenesis. J Embryol Exp Morphol 1983;78:83–125. [PubMed: 6663234]
52. Engler AJ, Sen S, Sweeney HL, Discher DE. Matrix elasticity directs stem cell lineage specification. Cell 2006;126:677–689. [PubMed: 16923388]
53. Netti PA, Berk DA, Swartz MA, Grodzinsky AJ, Jain RK. Role of extracellular matrix assembly in interstitial transport in solid tumors. Cancer Res 2000;60:2497–2503. [PubMed: 10811131]
54. Levick JR. Flow through Interstitium and Other Fibrous Matrices. Q J Exp Physiol Cogn Med Sci 1987;72:409–438.
55. Tang MD, Golden AP, Tien J. Molding of three-dimensional microstructures of gels. J Am Chem Soc 2003;125:12988–12989. [PubMed: 14570447]
56. Cabodi M, Cross VL, Qu Z, Havenstrite KL, Schwartz S, Stroock AD. An active wound dressing for controlled convective mass transfer with the wound bed. J Biomed Mater Res B Appl Biomater 2007;82:210–222. [PubMed: 17106898]
57. Perry, RH.; Green, DW. Chemical Engineers' Handbook. New York: McGraw-Hill; 1997.
58. Davis GE, Pintar Allen KA, Salazar R, Maxwell SA. Matrix metalloproteinase-1 and -9 activation by plasmin regulates a novel endothelial cell-mediated mechanism of collagen gel contraction and capillary tube regression in three-dimensional collagen matrices. J Cell Sci 2001;114:917–930. [PubMed: 11181175]
59. Stroock AD, Fischbach C. Microfluidic culture models of tumor angiogenesis. Tissue Eng Part A 2010;16:2143–2146. [PubMed: 20214470]

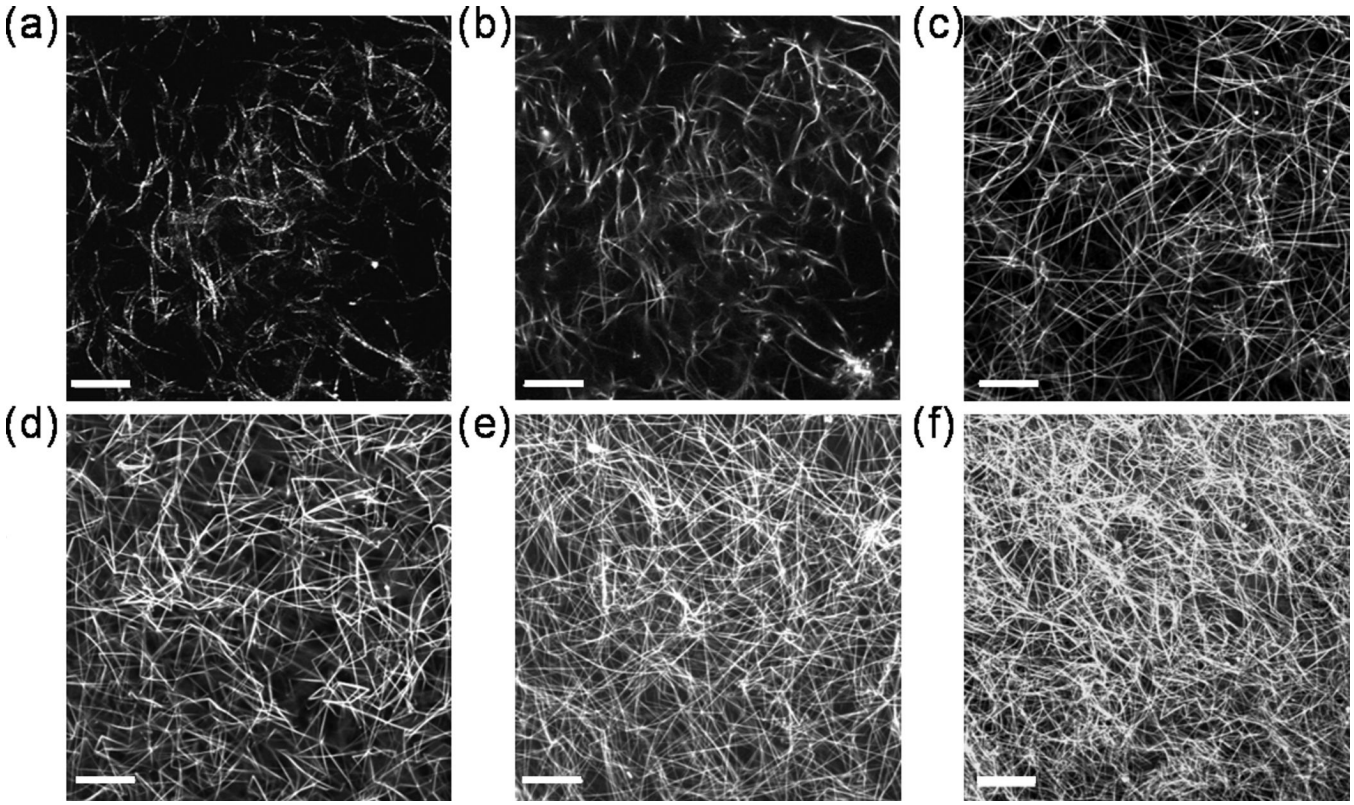

Fig. 1.

Structure of collagen fibers. **(a)** Reflectance confocal image of 0.3% collagen. **(b)** Fluorescence confocal image of 0.3% collagen. Fluorescence confocal images of **(c)** 0.8% **(d)** 1.0%, **(e)** 1.5%, and **(f)** 2.0% collagen. The images in (a) and (b) were of the same sample at the same location. Images are single, horizontal planes in hydrated, TRITC-labeled collagen gels acquired using a 63×, 1.4 NA oil immersion lens with pinhole = 1 Airy unit. Scale bars = 20 microns.

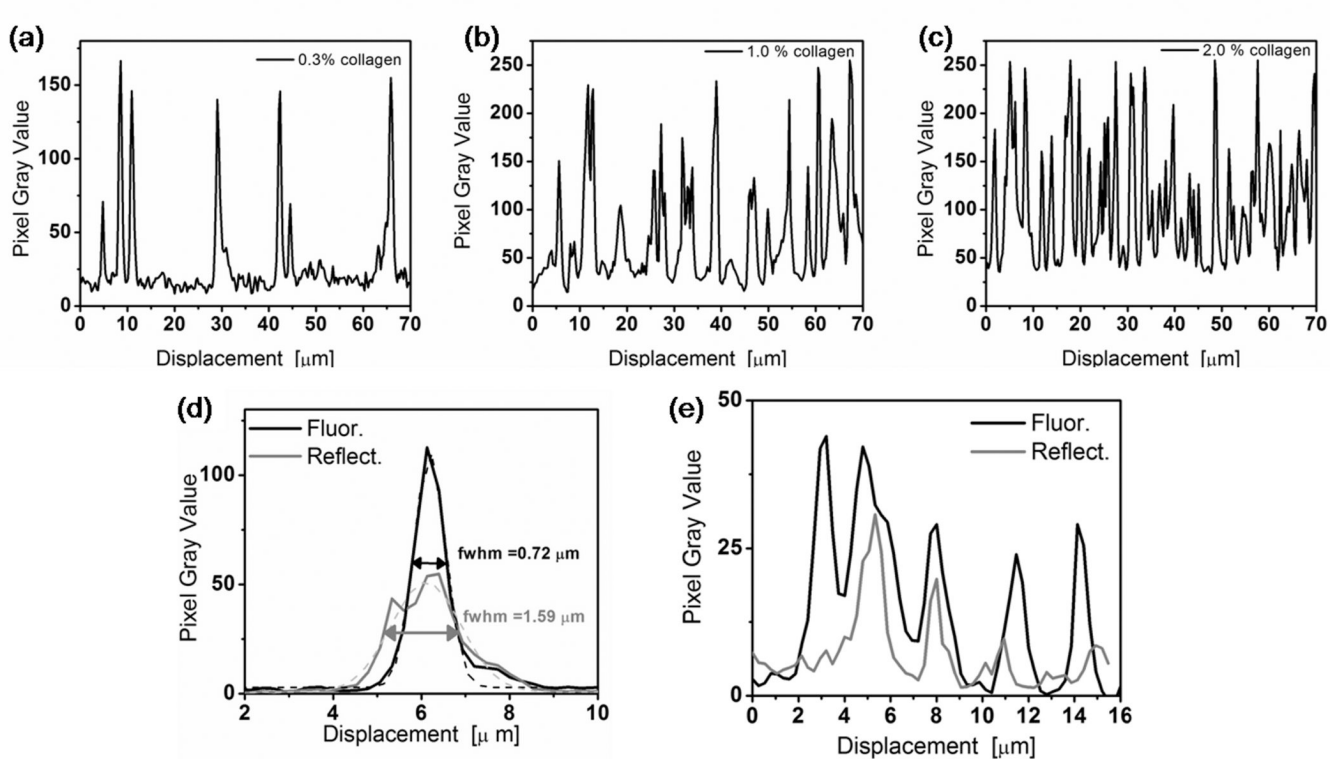

Fig. 2.

Quantification of fiber density and thicknesses in line scans from images in Fig. 1. Representative line scans across a 70 μm length of confocal fluorescence images from **(a)** 0.3%, **(b)** 1.0%, and **(c)** 2.0% uniform collagen. **(d)** Line scans from confocal reflectance (black line) and reflectance (grey line) images in Figs. 1a and 1b. The same lines were used for both the fluorescence and reflectance images. Local scans passed over a single fiber, perpendicular to its long axis. Intensity profiles were fit to a Gaussian distribution and full widths at half max (fwhm) are reported. **(e)** Extended scans across five essentially parallel fibers at the same location in images in Fig. 1 (a) and (b).

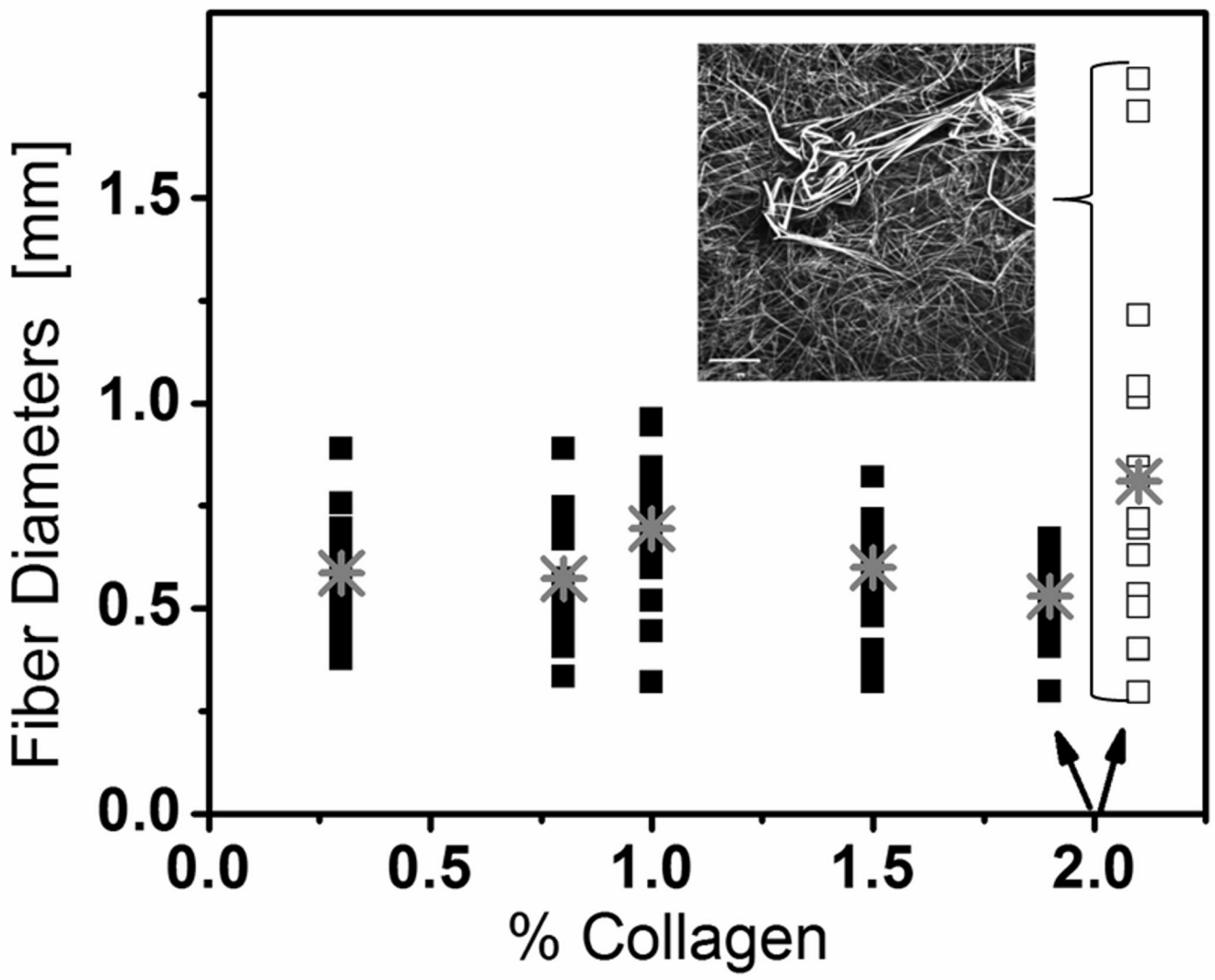

Fig. 3.

Summary of scans of single fiber line used to determine the average fiber diameter (gray cross point) for all collagen concentrations and a non-uniform 2.0% collagen gel (open squares and inset image). A total of 20 line scans were performed two separate samples for each collagen concentration.

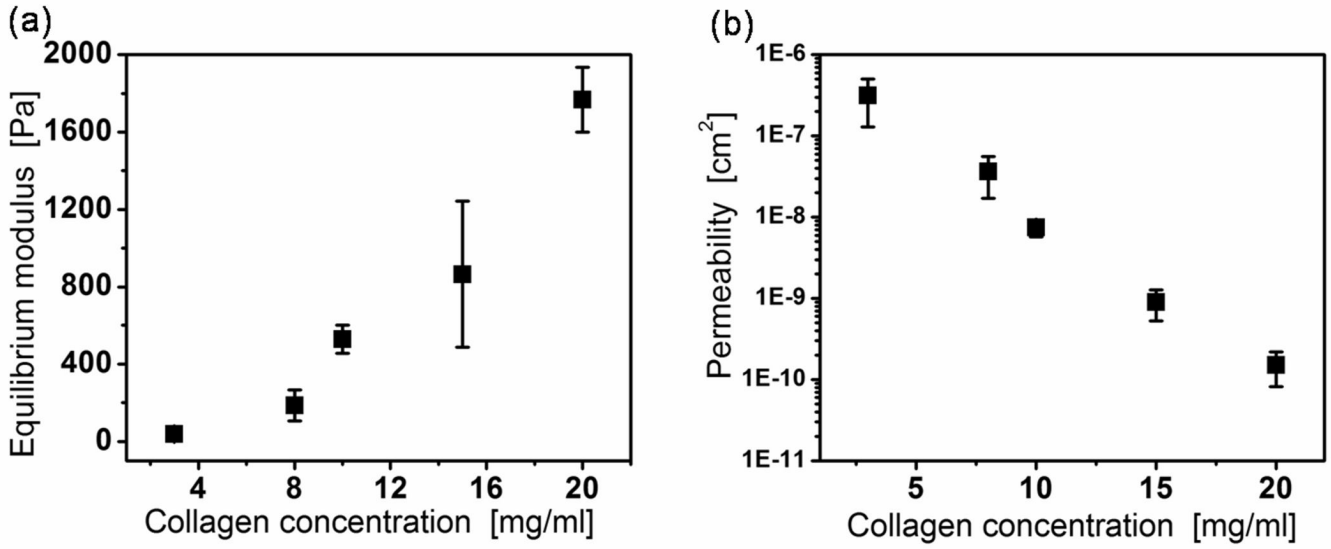

Fig. 4.

Mechanical properties of gels. **(a)** Equilibrium modulus, M_{eq} [Pa] and **(b)** hydraulic permeability, k [m^2/Pa*s] versus collagen concentration. Error bars represent the 95% confidence intervals from three samples compressed in increments of ~ 3% strain up to ~ 30% strain. Note logarithmic scale in (b). The permeability was obtained from the measured stress relaxation time constant and the equilibrium modulus, following reference [42].

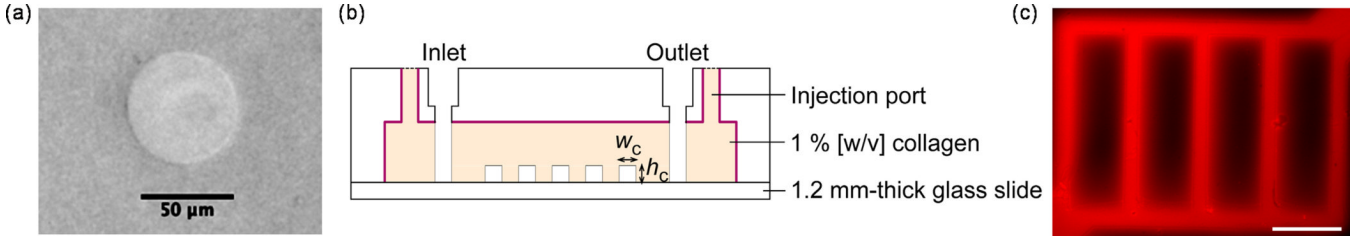

Fig. 5.

Microfabrication in dense collagen. **(a)** Replication of 50 µm-diameter pores in 0.3% gel. **(b)** Schematic illustration of fabricated and sealed microfluidic collagen. **(c)** Fluorescence micrograph of functional microfluidic 1 % [w/v] collagen during the delivery of RITC-dextran (70 kDa) via microchannels (scale bar = 500 µm; flow speed ~ 1 mm/s). Microchannel width, w_c was equal to microchannel height, h_c = 100 µm.

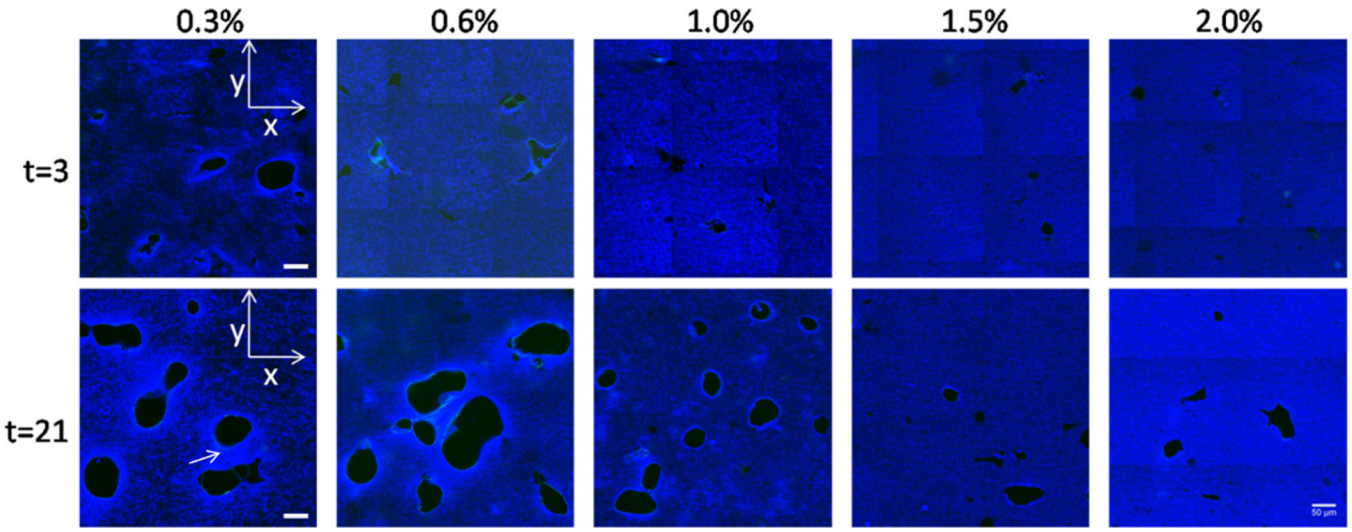

Fig. 6.

Confocal reflectance of collagen matrix during vasculogenesis. Confocal reflectance images at days 3 and 21 showing matrix-free lumens. Images show a single x-y plane ~ 20 μm above the adherent, bottom boundary. Void areas are are free of matrix and identified as capillary lumens. Using a 40× 1.3 NA oil immersion objective with a pinhole of 1 Airy Unit, a 3×3 array of images was taken using the automatic tile-scan function of the confocal microscope. Microscope software stitched the images together to form a single image. Arrow indicates brighter regions between cell structures. Scale bar = 50 μm.

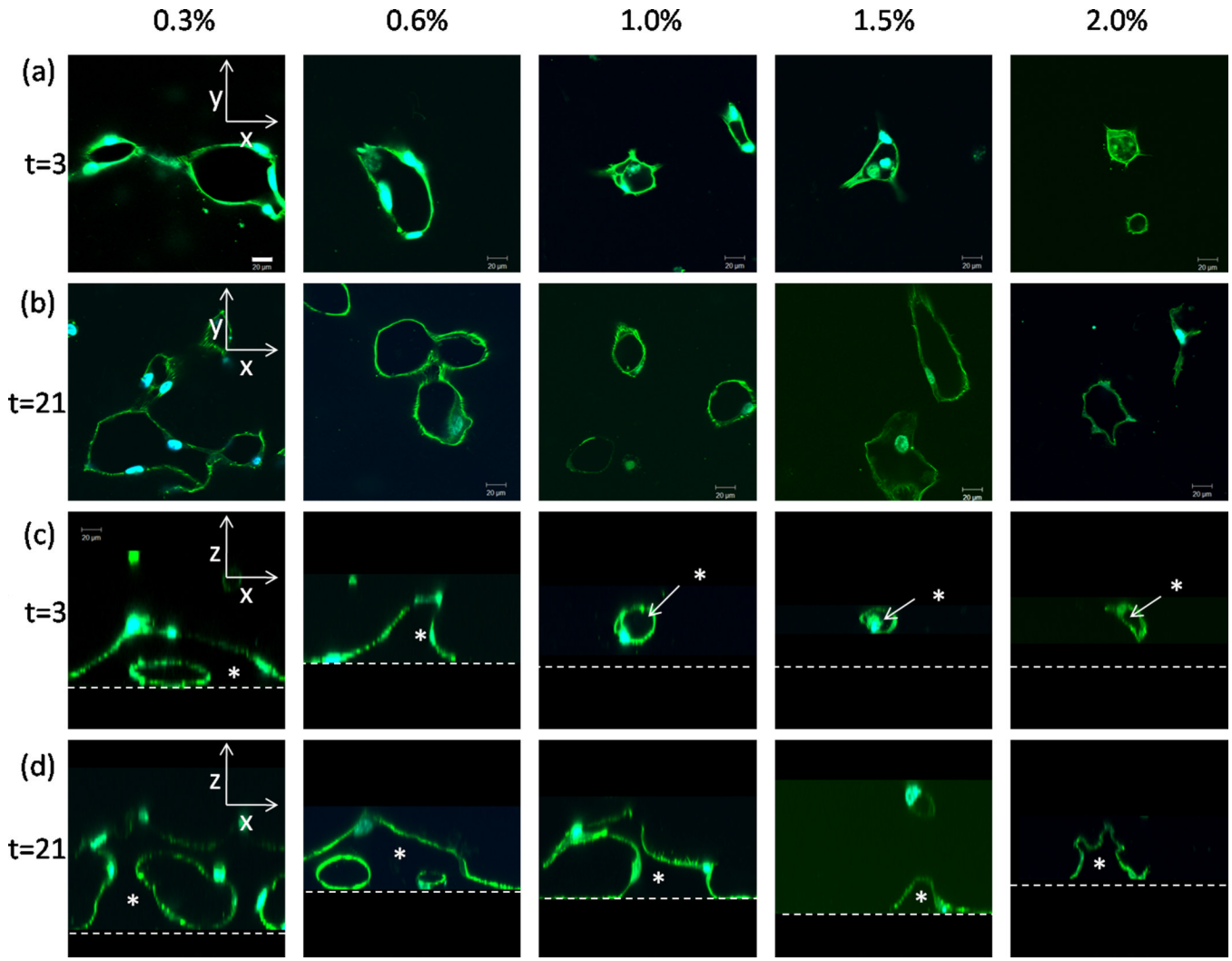

Fig. 7.

Endothelial lumen formation versus collagen concentration and time. **(a,b)** Confocal fluorescent images of a single *xy* plane ~ 20 microns above the bottom boundary at days 3 and 21. Cells were stained with Alexa Fluor−488 phalloidin and DAPI nuclear stain. Scale bar = 20 μm. **(c,d)** Confocal fluorescent images of *xz* cross-sections rendered from *z*-stacks through the collagen matrices at days 3 and 21. Dashed horizontal lines represent the location of the bottom boundary. Asterisks (*) indicate matrix-free lumens. Scale bar = 20 μm.

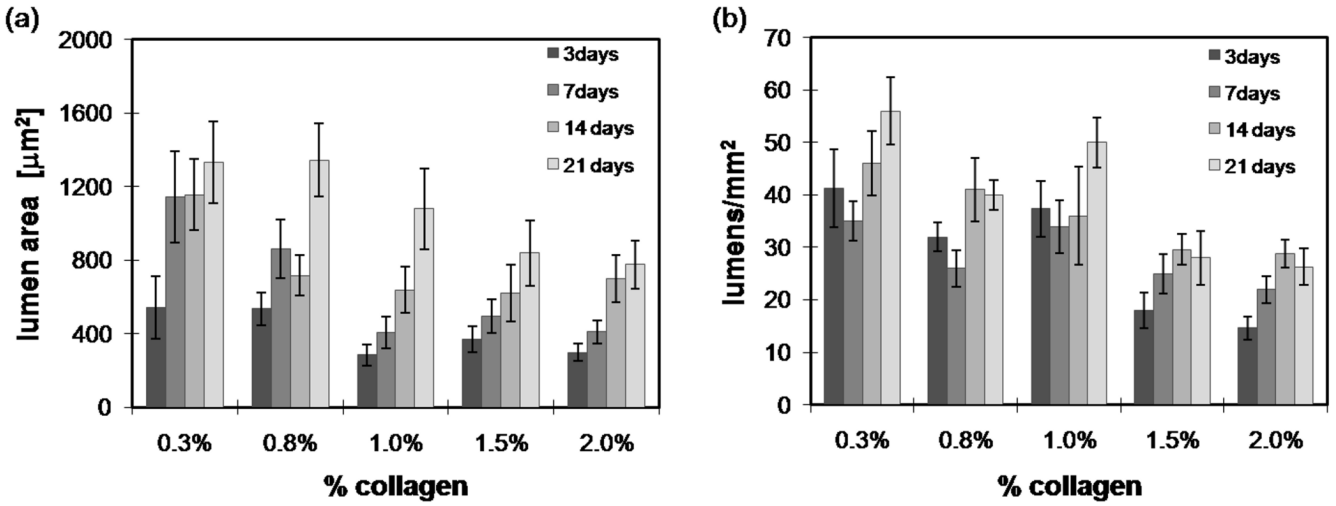

Fig. 8.

Quantification of lumen area and frequency. **(a)** Average lumen area and **(b)** average lumen frequency in the bulk ~20 microns from bottom boundary for various times and collagen concentrations. Collagen free lumens were quantified using confocal reflectance images with a total area of 0.25 mm^2. Images were made binary and lumen number and area were calculated using Image J. Error bars represent the standard deviation. n= 3–5 gels for each time point and condition.

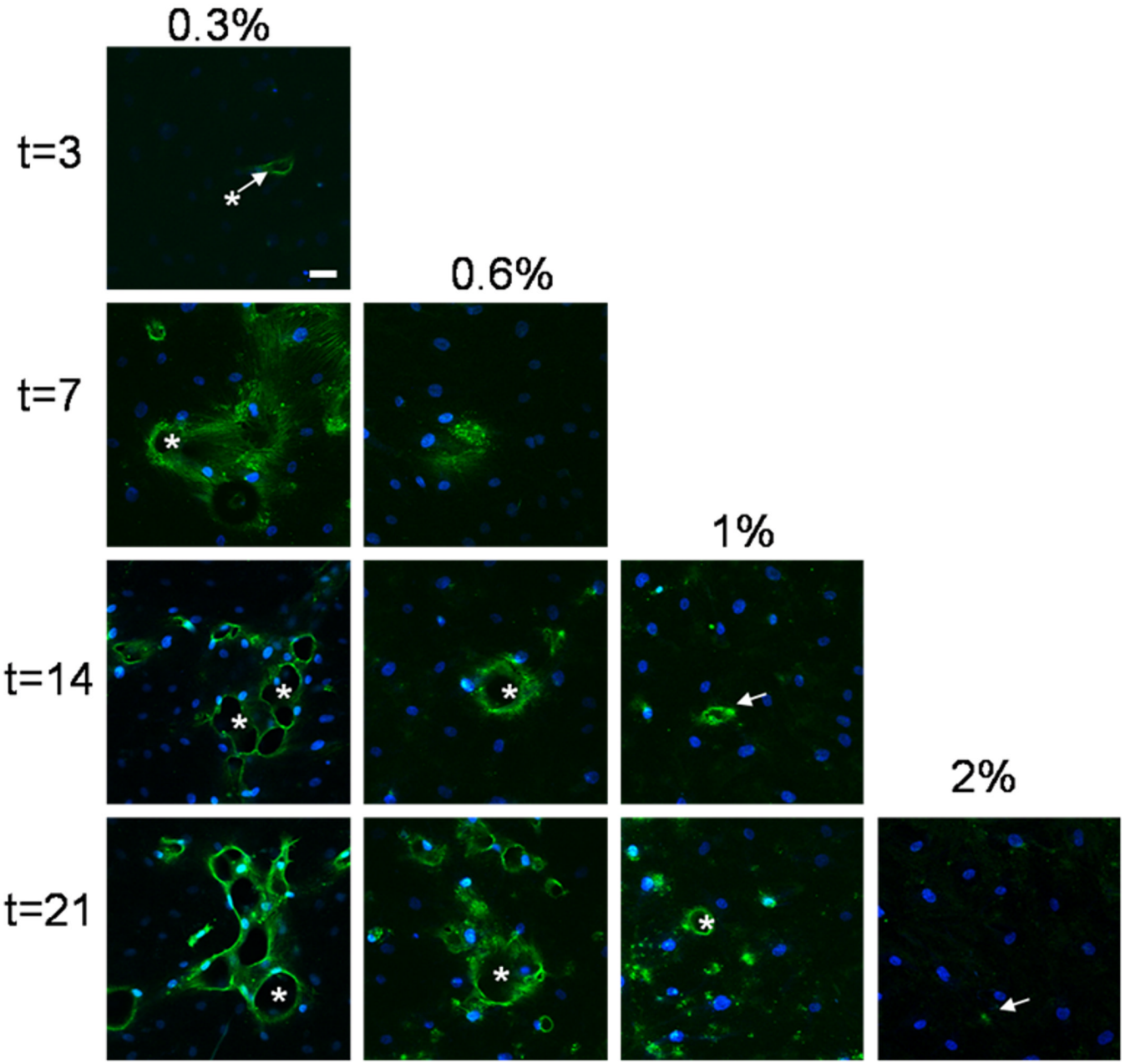

Fig. 9.

Distance and frequency of invasions versus collagen concentration and time. Confocal fluorescent images of single *xy* planes at $z = -10$ μm below the HUVEC monolayer at various time points for 0.3, 0.6, 1.0, and 2.0% collagen. Cells were stained with AlexaFluor 568 Phalloidin and YOYO-1 Iodide nuclear stain. Asterisks indicate open lumens. Arrows point to cellular structures. No images are included for the early time points for 0.6, 1.0%, and 2.0% collagen because no significant invasion had occurred. All images in this figure were taken using 20× objective with a pinhole of 1 Airy Unit. Scale bar = 50 μm.

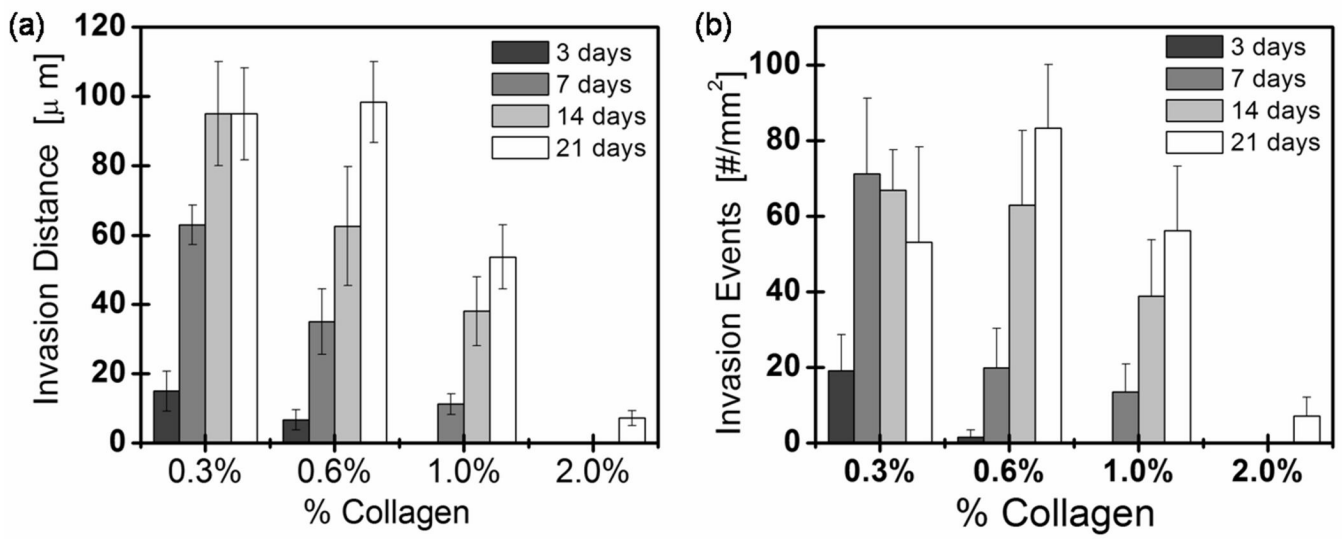

Fig. 10.

Quantification of lumen depth and frequency. **(a)** Invasion depth and **(b)** frequency into the collagen bulk at 3, 7, 14, and 21 days as a function of collagen concentration. Error bars represent the standard deviation n=3–5 gels for each time point and condition.

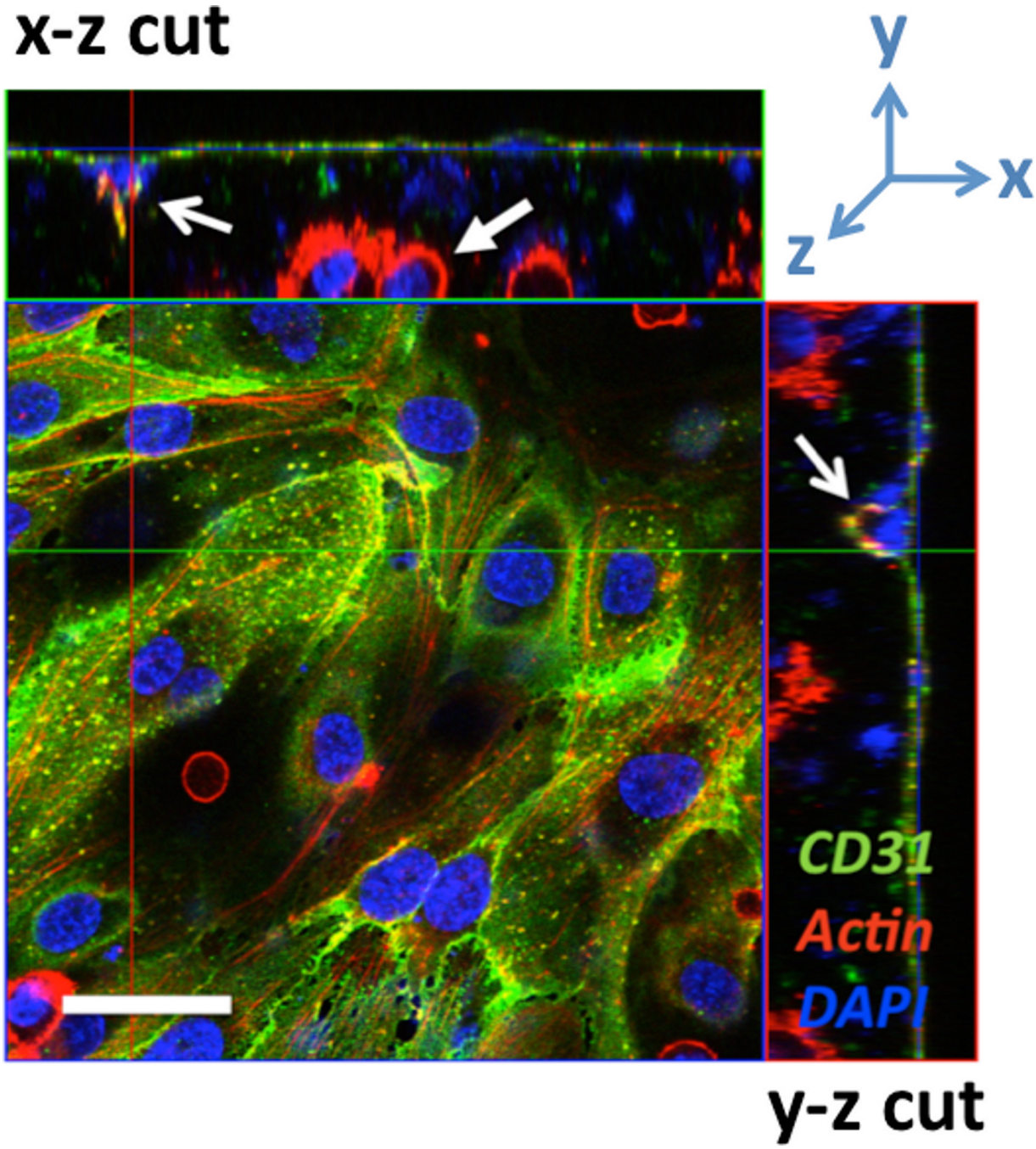

Fig. 11.

HUVEC and OSCC-3 co-culture. Fluorescent confocal micrograph demonstrating invasion of HUVECs from a surface monolayer into the bulk of an OSCC-3-seeded, 0.625% collagen scaffold at t=3 days. Samples are fixed and stained with DAPI (blue), AlexaFluor 568 phalloidin (red), and CD-31 mouse anti-human/AlexaFluor 488 goat anti-mouse (green). The two open arrows indicate the same HUVEC invasion event viewed in orthogonal cross-sections, while the solid arrow indicates a bulk OSCC-3 cell. Scale bar = 50 μm.

Table 1

Hydraulic pore radius, r_H was calculated using Carman-Kozeny model (Eq. 4). The geometric factor, k_{geo}, depends on the channel shape and the tortuosity. The average pore radius, a, was measured using confocal images of a single plane of fluorescently labeled fibers.

Collagen[mg/ml]	volume fraction, ϕ	porosity, ε	$k_{\parallel}$	$k_{\perp}$	k_{geo}	r_H [μm]	a [μm]	stdev (a)
3.0	0.006	0.994	157.965	83.1	108.1	58.7	14.5	3.7
8.0	0.015	0.985	100.932	39.6	60.0	15.0	9.5	4.3
10.0	0.019	0.981	95.736	33.7	54.3	6.5	7.1	1.9
15.0	0.028	0.972	95.772	25.2	48.7	2.0	2.2	0.7
20.0	0.038	0.962	110.847	20.7	50.7	0.9	1.1	0.5